Optics Letters

Stepped-height ridge waveguide MQW polarization mode converter monolithically integrated with sidewall grating DFB laser

Xiao Sun,[1,*] Weiqing Cheng,[1] Song Liang,[2] Shengwei Ye,[1] Yongguang Huang,[3] Ruikang Zhang,[3] Bocang Qiu,[4] Jichuan Xiong,[5] Xuefeng Liu,[5] John H. Marsh,[1] and Lianping Hou[1]

[1]James Watt School of Engineering, University of Glasgow, Glasgow G12 8QQ, UK
[2]College of Physics, Jilin University, Changchun 130012, China
[3]Institute of Semiconductors, Chinese Academy of Sciences, No. A35, East Qinghua Road, Haidian District, Beijing 100083, China
[4]Institute of Atomic and Molecular Science, Shaanxi University of Science and Technology, Xian 712081, China
[5]School of Electronic and Optical Engineering, Nanjing University of Science and Technology, Nanjing 210094, China
*Corresponding author: x.sun.2@research.gla.ac.uk

Received 20 October 2022; revised 17 November 2022; accepted 6 December 2022; posted 6 December 2022; published 4 January 2023

We report, to the best of our knowledge, the first demonstration of a 1555-nm stepped-height ridge waveguide polarization mode converter monolithically integrated with a sidewall grating distributed-feedback (DFB) laser using the identical epitaxial layer scheme. The device shows stable single longitudinal mode (SLM) operation with the output light converted from TE to TM polarization with an efficiency of >94% over a wide range of DFB injection currents (I_{DFB}) from 140 mA to 190 mA. The highest TM mode purity of 98.2% was obtained at $I_{DFB} = 180$ mA. A particular advantage of this device is that only a single step of metalorganic vapor-phase epitaxy and two steps of III-V material dry etching are required for the whole integrated device fabrication, significantly reducing complexity and cost.

https://doi.org/10.1364/OL.478765

Introduction. Polarization mode controllers (PMCs) are of increasing importance in numerous applications in optical communication systems to manipulate the TE–TM polarization state of light [1]. Frequency conversation in periodically poled lithium niobate (PPLN) waveguides requires TM polarized light while most semiconductor edge emitting lasers operate in TE polarization. There has been a growing interest in integrating PMCs with devices using multiple-quantum-well (MQW) structures as the active region, such as polarization-dependent phase shifters (PD-PSs) [2] and laser diodes (LDs) [3,4]. Previously reported PMCs based on MQW structures were able to convert pure TE- or TM-polarized light into an arbitrarily chosen state of polarization (SOP) but only with a 50% TE to TM polarization conversion efficiency (PCE) [2]. Despite the use of passive polarization control waveguides being well established in high-capacity data optical multiplexing systems, such as polarization division multiplexed (PDM) transmitters [5] and Stokes vector modulation direct detection (SVM-DD) transmitters [6], the realization of a monolithically integrated polarization controller and single longitudinal mode (SLM) light source, such as distributed feedback (DFB) laser, is significant. Although a PMC integrated with a 1550-nm Fabry–Perot (FP) LD has been reported in Ref. [3], the TE to TM PCE was only 80%. Until now there has been no report of a PMC integrated with a DFB laser. The crucial issue when integrating PMCs with MQW devices is the inherent birefringence of the MQW, which disturbs the optimal rotation of the SOP. The main mechanisms of SOP conversion in waveguides include the mode-coupling method [7], which exploits beating between two eigenmodes to enable polarization rotation along the PMC waveguide, and the mode-evolution method [8], which uses a change of the propagating mode inside the waveguide. The mode coupling approach to PMC design enables polarization conversion within a much shorter waveguide than the mode-evolution method. The mode coupling approach has therefore been proposed for integrating PMCs with MQW-based components such as LDs to reduce the internal loss caused by the strong exciton absorption inside the quantum well at the photoluminescence (PL) wavelength [9].

Several different PMC structures have been proposed such as waveguides using the reactive ion-etch (RIE) lag phenomenon [10], single-trench waveguides [11], angled-facet waveguides [12], and two-step waveguides [13]. These PMC devices use bulk material as the core layer in the waveguide and combine a high PCE with a short waveguide length. Nevertheless, relatively complicated butt-joint photonic integrated circuit (PIC) techniques involving re-growth are usually used to integrate PMCs with MQW-based devices. To simplify the monolithic fabrication, we have proposed an InP-AlGaInAs MQW-based sidewall grating (SWG) DFB laser with a stepped height waveguide PMC [14]. An optimized epitaxial design was proposed for integrating the DFB laser with the PMC waveguide. A series of full-wave simulations have been made to

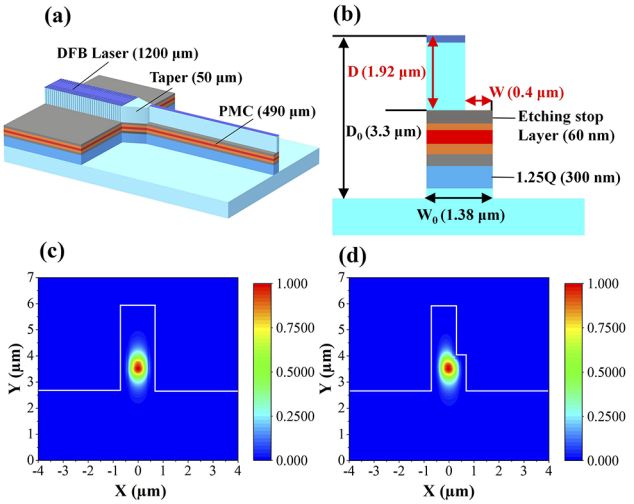

Fig. 1. (a) Schematic of the monolithic DFB-PMC device, (b) cross section structure of the PMC; the fundamental eigenmodes (c) in the taper tip cross section and (d) in the PMC stepped-height ridge waveguide.

optimize the geometric parameters of PMC to obtain a high TE-TM PCE.

In this work, based on our simulation work in Ref. [14], an AlGaInAs MQW SWG DFB laser was fabricated and monolithically integrated with a stepped waveguide PMC based on the identical epitaxial layer (IEL) integration scheme for the first time, to the best of our knowledge. This approach needs only a single step of metalorganic vapor-phase epitaxy (MOVPE) and two steps of III-V material etching. Compared with the conventional buried grating DFB lasers, the SWG DFB laser avoids the complicated etch and regrowth processes required to complete the laser structure after the grating definition. Compared with the butt-joint and selective area growth (SAG) PIC technologies, the IEL integration scheme eliminates time-consuming etch and regrowth steps. The DFB-PMC device reported here operates in a stable SLM and has a high PCE (>94%) over a wide range of DFB injection currents. The highest PCE obtained was 98.2%, which is consistent with the simulation results.

Device design and fabrication. The wafer structure used for the DFB-PMC is the same as that described previously [14]. This wafer contains five 6-nm-thick compressively strained (+1.2%) AlGaInAs quantum wells (QWs) and six 10-nm-thick tensile strained (–0.3%) AlGaInAs quantum barriers (QBs). The room temperature PL peak of the QWs was located at a wavelength of 1530 nm. An optimized 300-nm-thick 1.25Q (1.25Q means the PL wavelength of this material is 1.25 μm) layer is embedded below the MQW layer to increase the difference between the propagation constants of the two fundamental modes of the PMC so reducing the half-beat length (L_π) and increasing the PCE. The schematic of the DFB-PMC device is depicted in Fig. 1(a). It comprises a 1200-μm-long shallow etched SWG DFB laser, a 50-μm-long deep etched taper, and a 490-μm-long PMC waveguide. The width of the taper is changed from 2.5 μm to 1.38 μm to facilitate the TE mode transition to the PMC and prevent the generation of multiple transverse modes. The simulated reflection between the shallow etched DFB and deep etched taper sections is approximately 7×10^{-6}, which will have a negligible impact on DFB performance. The simulation also shows the excess optical loss of the taper is 1%, i.e.,

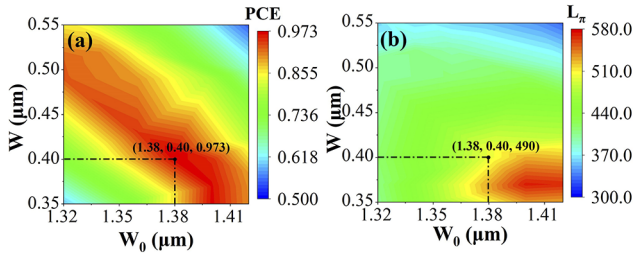

Fig. 2. (a) Calculated maximum PCE and (b) corresponding L_π as a function of waveguide width (W_0) and corner width (W).

0.044 dB, which includes the scattering and mode mismatch losses, and can also be neglected. The ridge waveguide of the DFB is 2.5 μm wide and 1.92 μm high. The grating period is 238 nm with a grating recess depth of 0.6 μm giving a 1.55-μm Bragg wavelength. The grating coupling coefficient κ was measured to be approximately 15 cm^{-1} using the equation in Ref. [15]. A quarter wavelength shift section was inserted at the center of the DFB laser cavity to ensure SLM oscillation. The stepped-height PMC consisted of a ridge profile where W_0 and W are the widths of the ridge waveguide and dry-etch corner, and D_0 and D are the deep and shallow dry etched depths, respectively. Here, $D_0 = 3.3$ μm and $D = 1.92$ μm were chosen for the PMC waveguide as presented in Fig. 1(b). The D is the same as the DFB laser ridge height and can be precisely controlled because the 60-nm-thick cladding AlGaInAs waveguide layer on top of the MQW layers acts as a dry etch stop layer when using a $CH_4/H_2/O_2$ recipe in an inductively coupled plasma (ICP) dry etch tool. To optimize the PMC width, a Full-Wave simulation was made using an FDTD software package. Figures 1(c) and 1(d) present the fundamental modes inside the taper tip cross section and PMC waveguide. The PMC eigenmode is optimized to rotate the electric/magnetic fields through 45°. After propagating a half-beat length $L_\pi = \pi/(\beta_1 - \beta_2)$ (where β_1 and β_2 are the propagation constants of the TE and TM eigenmodes, respectively), the polarization is rotated through 90°, and the output mode becomes TM-polarized. The calculated effective modal indexes (N_{eff}) of the fundamental TE and TM modes in the PMC waveguide are 3.21109 and 3.20951, respectively. Figure 2 shows a contour plot of the calculated PCE and L_π as a function of W_0 and W. The final optimum widths of the PMC waveguide chosen here are $W_0 = 1.38$ μm and $W = 0.4$ μm, which provide a high PCE (97.3%) and short L_π (490 μm). The DFB-PMC fabrication process is presented in Fig. 3. The wafer is grown on an InP substrate by MOVPE [Fig. 3(a)]. The DFB grating and PMC first step shallow etched waveguide pattern is defined by e-beam lithography (EBL) using negative tone hydrogen silsesquioxane (HSQ) photoresist which acts as both an EBL resist and ICP dry etching hard mask in Fig. 3(b). In Fig. 3(c), the ridge is first etched to a depth of 1.89 μm in an ICP system using a $Cl_2/CH_4/H_2/Ar$ gas mixture, where the etching rate for InP, InGaAsP, and AlGaInAs is approximately 182 nm/minute. Then, the gas recipe was changed to $CH_4/H_2/O_2$ and the ridge waveguide was continuously etched to a height of 1.92 μm, with an etch rate for InP and InGaAsP of approximately 78 nm/minute, while that of the upper 60-nm AlGaInAs layer was 3 nm/minute, which is a 26-fold selectivity with respect to InGaAsP and InP. After the shallow ridge waveguide was etched, both the DFB grating and PMC's first step waveguide were protected using HSQ, and the second PMC deep etched

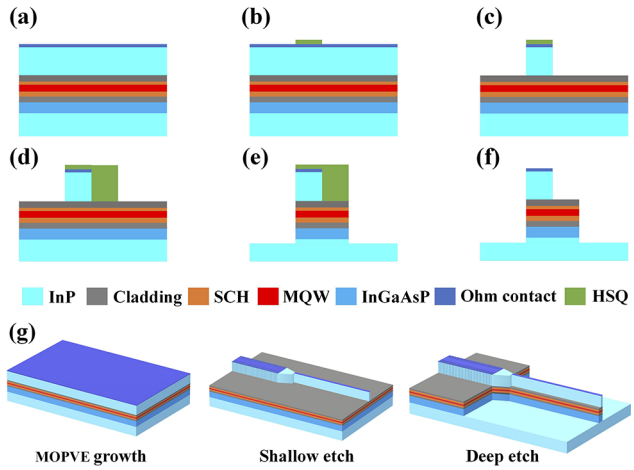

Fig. 3. Fabrication procedures: (a) MOVPE wafer; (b) EBL to write the laser and PMC first step waveguide; (c) ICP shallow etching; (d) EBL to write the second step waveguide of PMC; (e) ICP deep etching; (f) HSQ strip off; (g) workflow of the monolithic DFB-PMC device fabrication.

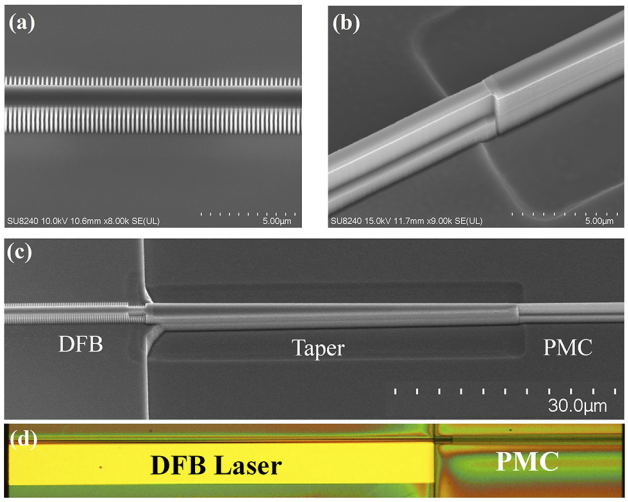

Fig. 4. (a) SEM image of DFB SWGs, (b) SEM image at the interface between PMC and taper, (c) SEM images of DFB-PMC device, (d) microscope picture of the DFB -PMC device.

ridge waveguide was defined by EBL, as shown in Fig. 3(d). A second ICP etch with $Cl_2/CH_4/H_2/Ar$ was used to etch the PMC ridge waveguide to a height of 3.3 μm [Fig. 3(e)]. Finally, the HSQ resist was removed with hydrofluoric acid, as shown in Fig. 3(f). The fabrication workflow is depicted in Fig. 3(g); only a single step of MOVPE and two steps of dry etching are required for the whole integrated device. SEM images of the DFB grating, taper, and PMC waveguide are presented in Figs. 4(a)–4(c). The subsequent deposition of SiO_2 and HSQ passivation layers, SiO_2 window opening, P-contact deposition, substrate thinning, and N-contact deposition are the same as for conventional LD fabrication and can be referred to Ref. [16]. An optical microscopy picture of the completed DFB-PMC device is depicted in Fig. 4(d). Finally, the devices were mounted epilayer up on a copper heat sink on a Peltier cooler. The heat sink temperature was set at 20°C and the devices were tested under CW conditions.

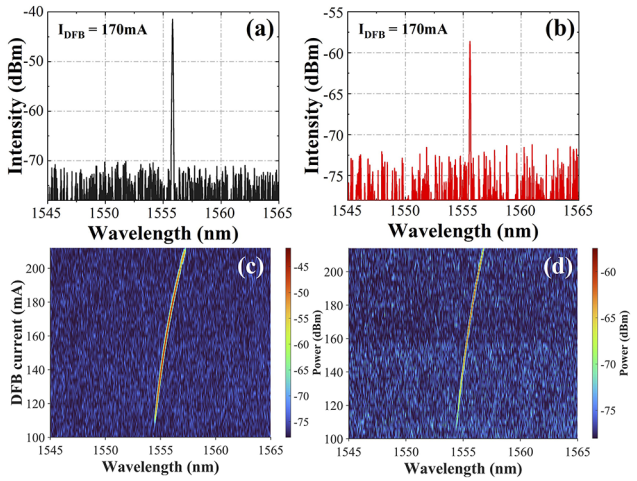

Fig. 5. Measured optical spectrum from (a) DFB LD rear facet and (b) PMC section output facet at 170 mA. 2D optical spectrum at (c) DFB LD rear facet and (d) PMC section output facet.

Device measurements. The measured internal loss for the PMC waveguide at 1550-nm wavelength is 9/cm. Figure 5(a) shows the optical spectrum from the rear side of the DFB section at $I_{DFB} = 170$ mA. The spectrum was measured with a resolution bandwidth (RBW) of 0.06 nm. The peak lasing wavelength is 1555.81 nm with a side mode suppression ratio (SMSR) of at least 29 dB, the measurement of which is limited by the amount of power coupled into the lensed fiber from the rear side of the DFB LD.

Figure 5(b) presents the optical spectrum from the PMC section output side. The attenuation of output power at the PMC facet is due to the strong exciton absorption inside the PMC waveguide when the propagating light wavelength is close to the PL wavelength of the MQW core (1530 nm). Figures 5(c) and 5(d) present 2D optical spectra measured from the DFB rear side and PMC output side, respectively, over a range of I_{DFB} from 100 mA to 220 mA. There is stable SLM operation over a wide range of I_{DFB} without any longitudinal mode hops. The threshold current, I_{DFB}, is 104 mA. The average current-induced wavelength redshift coefficient was found to be 0.020 nm/mA. The setup of the SOP measurement is shown in Fig. 6(a). The DFB-PMC device was mounted on a thermoelectric cooler (TEC) and temperature controlled at 20°C, as stated previously. The output light from the PMC was coupled to a lensed polarization-maintaining (PM) fiber and transmitted to a polarimeter to measure the SOP. Both the current driver and the polarimeter were controlled by a computer through the general-purpose interface bus (GPIB) interface. First, the SOP from the DFB laser rear facet was measured at I_{DFB} from 104 mA to 210 mA, and the Stokes vector was constant at $(S_1, S_2, S_3) = (0.998, 0.05, 0.04)$, where S_1, S_2, S_3 are the S-parameters of the SOP. As expected, the light was TE-polarized with a purity of 99.8%. The SOP at the PMC section output facet is depicted in Fig. 6(b). The S_1 parameter was found to be <-0.94 within the range $140\text{ mA} < I_{DFB} < 190\text{ mA}$. Outside this this range, the S_1 parameter remained at <-0.8. This is because the SMSR from the PMC output facet is lower than the SMSR sensitivity of the polarimeter when I_{DFB} is <140 mA or >190 mA. The maximum S_1 is detected at $I_{DFB} = 180$ mA where the SOP is (–0.982, 0.08, 0.17) representing a TM purity of 98.2%. This result is nearly the same as the simulated PCE of 97.3%. Figure 6(c) shows the SOP on

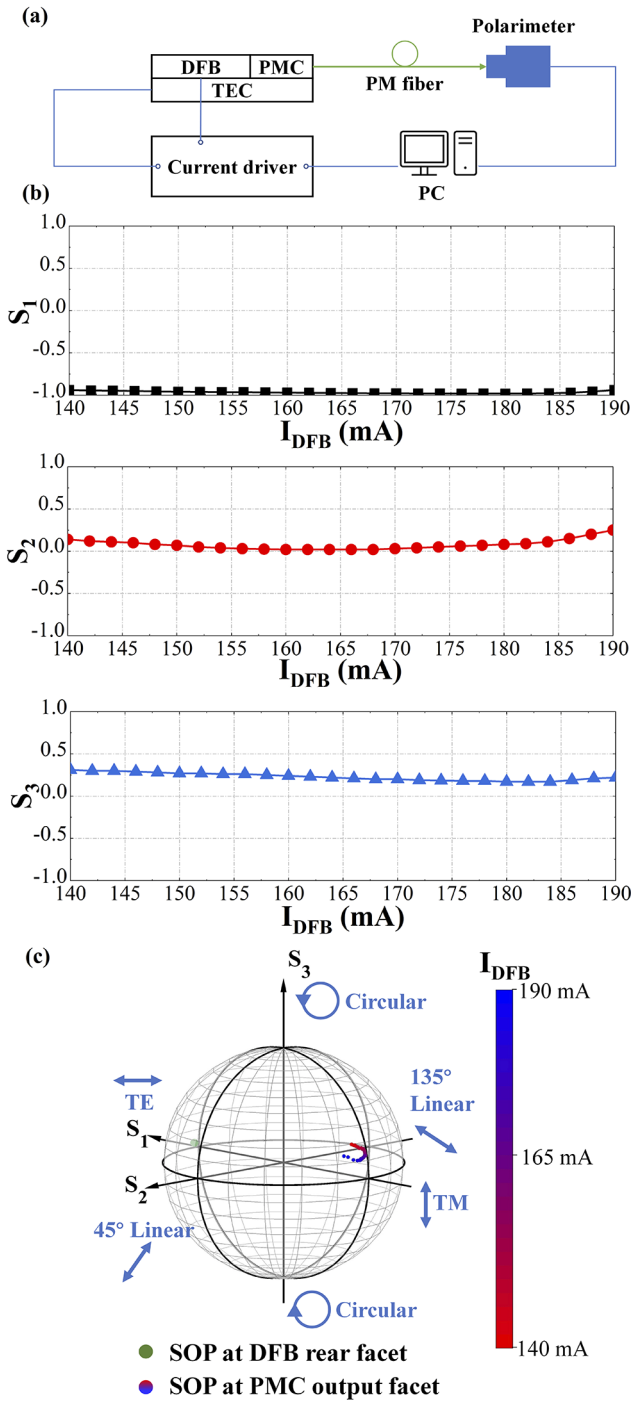

Fig. 6. (a) SOP measurement setup, (b) S-parameters of the SOP at PMC output facet side as a function of I_{DFB}, (c) SOP on the Poincaré sphere with I_{DFB} from 140 mA to 190 mA.

the Poincaré sphere for the DFB laser rear facet and the PMC output facet with I_{DFB} = (140–190) mA. The SOP at I_{DFB} = 140 mA corresponds to the inside point of the "U" shape curve on the Poincaré sphere. The 4.0% deviation of the measured SOP is due to the measurement errors caused by the noise of the DC source driving the DFB laser, and environmental influences such as temperature fluctuations and mechanical vibration.

We note the fabricated PMC length should be kept as close as possible to the designed value by precise control of the cleaving. Here, a LOOMIS LSD-100 cleaving tool was used with a cleaving accuracy of ±1 μm. The resulting variation in the PCE is less than 0.1%, confirming the tool meets the required tolerance. We also comment that to increase the output power of the device, quantum well intermixing (QWI) could be used to blueshift the bandgap in the PMC section and reduce its absorption loss.

Conclusion. A novel monolithically integrated DFB-PMC device has been fabricated based on an SWG and IEL structure for the first time, to the best of our knowledge. The PMC is designed as a stepped height ridge waveguide. A major advantage of the design is that only a single MOVPE step and two dry-etch steps are required to fabricate the device. The device operates in a stable SLM with a current-induced wavelength redshift coefficient of 0.020 nm/mA. The PMC has a high TM purity (>94%) over a wide I_{DFB} range (140–190 mA), and a maximum TM mode purity of 98.2% was measured at I_{DFB} = 180 mA.

Funding. Engineering and Physical Sciences Research Council (EP/R042578/1); Chinese Ministry of Education Collaborative Project (B17023).

Acknowledgments. We would like to acknowledge the staff of the James Watt Nanofabrication Centre at the University of Glasgow for their help in fabricating the devices.

Disclosures. The authors declare no conflict of interest.

Data availability. Data underlying the results presented in this paper are not publicly available at this time but may be obtained from the authors upon reasonable request.

REFERENCES

1. P. J. Winzer, D. T. Neilson, and A. R. Chraplyvy, Opt. Express **26**, 24190 (2018).
2. M. Ito, K. Okawa, T. Suganuma, T. Fukui, E. Kato, T. Tanemura, and Y. Nakano, Opt. Express **29**, 10538 (2021).
3. B. Holmes, M. Naeem, D. Hutchings, J. Marsh, and A. Kelly, Opt. Express **20**, 20545 (2012).
4. J. Bregenzer, S. McMaster, M. Sorel, B. Holmes, and D. Hutchings, presented at the *Conference on Lasers and Electro-Optics* (2008).
5. S. An and O. K. Kwon, Opt. Express **26**, 1305 (2018).
6. D. Che and W. Shieh, J. Lightwave Technol. **34**, 754 (2016).
7. A. E. Elfiqi, R. Kobayashi, R. Tanomura, T. Tanemura, and Y. Nakano, IEEE Photonics Technol. Lett. **32**, 663 (2020).
8. A. E. Elfiqi, R. Tanomura, D. Yu, W. Yanwachirakul, H. Shao, Y. Suzuki, T. Tanemura, and Y. Nakano, IEEE Photonics Technol. Lett. **34**, 109 (2022).
9. X. Sun, W. Cheng, Y. Sun, S. Ye, A. Al-Moathin, Y. Huang, R. Zhang, S. Liang, B. Qiu, and J. Xiong, Photonics **9**, 564 (2022).
10. B. Holmes and D. Hutchings, IEEE Photonics Technol. Lett. **18**, 43 (2006).
11. S.-H. Kim, R. Takei, Y. Shoji, and T. Mizumoto, Opt. Express **17**, 11267 (2009).
12. U. Khalique, Y. C. Zhu, J. J. G. M. van der Tol, L. M. Augustin, R. Hanfoug, F. H. Groen, P. J. van Veldhoven, M. K. Smit, M. van de Moosdijk, W. de Laat, and K. Simon, presented at the *Integrated Photonics Research and Applications/Nanophotonics for Information Systems*, San Diego, California, 10 April2005.
13. C. Alonso-Ramos, S. Romero-García, A. Ortega-Moñux, I. Molina-Fernández, R. Zhang, H. Bach, and M. Schell, Opt. Lett. **37**, 335 (2012).
14. X. Sun, S. Ye, W. Cheng, S. Liang, Y. Huang, B. Qiu, Z. Li, J. Xiong, X. Liu, J. H. Marsh, and L. Hou, IEEE Photonics J. **14**, 1 (2022).
15. M. Razeghi, R. Blondeau, M. Krakowski, J.-C. Bouley, M. Papuchon, B. Cremoux, and J. Duchemin, IEEE J. Quantum Electron. **21**, 507 (1985).
16. L. Hou, M. Tan, M. Haji, I. Eddie, and J. H. Marsh, IEEE Photonics Technol. Lett. **25**, 1169 (2013).